THE REALGAS AND REALGASH2O OPTIONS OF THE TOUGH+ CODE FOR THE SIMULATION OF COUPLED FLUID AND HEAT FLOW IN TIGHT/SHALE GAS SYSTEMS

George J. Moridis, C. Matthew Freeman, Stephen Webb and Stefan Finsterle

Lawrence Berkeley National Laboratory
1 Cyclotron Rd.
Berkeley, CA, 94706, USA
e-mail: GJMoridis@lbl.gov

ABSTRACT

We developed two new EOS additions to the TOUGH+ family of codes, the RealGasH2O and RealGas. The RealGasH2O EOS option describes the non-isothermal two-phase flow of water and a real gas mixture in a gas reservoir (including a tight/shale gas one). The gas mixture is treated as either a single-pseudo-component having a fixed composition, or as a multicomponent system composed of up to 9 individual real gases. The RealGas option has the same general capabilities, but does not include water, thus describing a single-phase, dry-gas system. The capabilities of two codes include: coupled flow and thermal effects in porous and/or fractured media, real gas behavior, inertial (Klinkenberg) effects, full micro-flow treatment, Darcy and non-Darcy flow through the matrix and fractures of fractured media, gas sorption onto the grains of the porous media, etc.

The codes are verified against available analytical and semi-analytical solutions. Their capabilities are demonstrated in a series of problems of increasing complexity, ranging from isothermal flow in simpler 1D and 2D conventional gas reservoirs, to non-isothermal gas flow in 3D fractured shale gas reservoirs involving 4 types of fractures, micro-flow, non-Darcy flow and gas composition changes during production.

INTRODUCTION

Background

TOUGH+ is a family of codes developed at the Lawrence Berkeley National Laboratory (Moridis et al., 2008) that are a successor to the TOUGH2 (Pruess et al., 1991) family of codes for multi-component, multiphase fluid and heat flow. It is written in standard FORTRAN 95/2003 to take advantage of all the object-oriented capabilities and the enhanced computational features of that language. It employs dynamic memory allocation, follows the tenets of Object-Oriented Programming (OOP), and involves entirely new data structures and derived data types that describe the objects upon which the code is based. The TOUGH+ code is based on a modular structure that is designed for maximum traceability and ease of expansion.

Objective

The main objective of this study was to develop numerical capabilities allowing the description of a wide range of processes involved in the non-isothermal flow through the spectrum of natural gas reservoirs in geologic systems, including tight-gas and shale-gas reservoirs with natural and/or induced fractures. To that end, we developed two new EOS additions to the TOUGH+ family of codes: the RealGasH2O and RealGas options for the description of two-phase (aqueous and gas) and single-phase (dry-gas) flow through complex geologic media, respectively. Although the new capabilities can provide solutions to the problem of prediction of gas production from the entire spectrum of gas-bearing reservoirs, of particular interest are applications to tight-sand and shale reservoirs, the numerical simulation of which may involve extremely fine domain discretization, complex fracture-matrix interactions in several subdomains of the producing system, and coupled thermophysical phenomena and processes.

CODE DESCRIPTION

The ensuing discussion focuses on the description of the TOUGH+RealGasH2O code (hereafter referred to as T+GW) describing the two-phase flow problem of an aqueous and a gas phase flow through a geologic system. The TOUGH+RealGas code (hereafter referred to as T+G) is entirely analogous, differing only in the

omission of water as a mass component, thus solving the much simpler problem of single-phase, dry-gas flow and production.

Fundamental Equations of Mass and Energy Balance

A non-isothermal fractured tight-gas or shale-gas system can be fully described by the appropriate mass balance equations and an energy balance equation. The following components κ, corresponding to the number of equations, are considered: $\kappa = g^i$, i.e., the various gaseous components (compounds) i constituting the natural gas ($i = 1, \ldots, N_G$, $N_G \geq 1$); water (w), and heat (θ), treated as a pseudo-component. Note that in T+GW it is possible to treat a real gas mixture of constant composition (i.e., with non-variant mole fractions Y^i) as a *single pseudo-component*, the properties of which vary with the pressure P and temperature T.

Following Pruess et al. (1999), mass and heat balance considerations in every subdomain (gridblock) into which the simulation domain is been subdivided by the integral finite difference method in TOUGH+ dictates that

$$\frac{d}{dt}\int_{V_n} M^\kappa dV = \int_{\Gamma_n} \mathbf{F}^\kappa \cdot \mathbf{n}\, dt + \int_{V_n} q^\kappa dV \qquad (1)$$

where V, V_n are the volume and volume of subdomain n [m^3]; M^κ is the mass accumulation term of component κ [kg m^{-3}]; A, Γ_n are the surface area and surface of subdomain n [m^2], respectively; $\mathbf{F}^\kappa$ is the flow vector of component κ [kg $m^{-2}s^{-1}$]; $\mathbf{n}$ is the inward unit normal vector; q^κ is the source/sink term of component κ [kg $m^{-3}s^{-1}$]; and t is the time [s].

Mass accumulation terms

Under the two-phase (aqueous and gas) flow conditions described by T+GW, the mass accumulation terms M^κ for the mass components κ in equation (1) are given by

$$\sum_{\beta=A,G} \phi\, S_\beta \rho_\beta X_\beta^\kappa + \delta_\Psi (1-\phi)\rho_R \Psi^i \qquad (2)$$

where $\kappa \equiv w, g^i,\ i = 1, \ldots, N_G$; ϕ is the porosity [*dimensionless*]; ρ_β is the density of phase β [kg m^{-3}]; S_β is the saturation of phase β [*dimensionless*]; X_β^κ is the mass fraction of component in phase β [kg/kg]; ρ_R is the rock density [kg m^{-3}]; Ψ^i is the mass of sorbed component g^i per unit mass of rock [kg/kg]; and $\delta_S = 0$ for non-sorbing media (including tight-gas systems) that are usually devoid of substantial organic carbon, while $\delta_S = 1$ in gas-sorbing media such as shales.

The first term in equation (2) describes fluid mass stored in the pores, and the second the mass of gaseous components sorbed onto the organic carbon (mainly kerogen) content of the matrix of the porous medium. The latter is quite common in shales. Although gas desorption from kerogen has been studied extensively in coalbed CH_4 reservoirs, and several analytic/semi-analytic models have been developed for such reservoirs (Clarkson and Bustin, 1999), the sorptive properties of shale are not necessarily analogous to coal (Schettler and Parmely, 1991).

Gas sorption terms

The most commonly used empirical model describing sorption onto organic carbon in shales is analogous to that used in coalbed methane and follows the Langmuir isotherm that, for a single-component gas, is described by

$$\begin{cases} \Psi^i = \dfrac{p_{dG} m_L}{p_{dG} + p_L} & \text{for ELaS} \\ \dfrac{d\Psi^i}{dt} = k_L \left(\dfrac{p_{dG} m_L}{p_{dG} + p_L} - \Psi^i \right) & \text{for KLaS} \end{cases} \qquad (3)$$

where p_{dG} is the dry gas pressure, ELaS indicates Equilibrium Langmuir Sorption, and KLaS denotes Kinetic Langmuir Sorption. The m_L term in equation (3) describes the total mass storage of component g^i at infinite pressure (kg of gas/kg of matrix material), p_L is the pressure at which half of this mass is stored (Pa), and k_L is a kinetic constant of the Langmuir sorption (1/s). In most studies applications, an *instantaneous equilibrium* is assumed to exist between the sorbed and the free gas, i.e., there is no transient lag between pressure changes and the corresponding sorption/desorption responses and the equilibrium model of Langmuir sorption is assumed to be valid (Figure 6). Although this appears to be a good approximation in shales (Gao et al., 1994) because of the very low permeability of the matrix (onto which the various gas components are sorbed), the subject has not been fully investigated. For multi-component gas, equation (3) becomes

$$\begin{cases} \Psi^i = \dfrac{p_{dG} B^i m_L^i \Upsilon^i}{1 + p_{dG} \sum_i B^i \Upsilon^i} & \text{for ELaS} \\ \dfrac{d\Psi^i}{dt} = k_L^i \left(\dfrac{p_{dG} B^i m_L^i \Upsilon^i}{1 + p_{dG} \sum_i B^i \Upsilon^i} - \Psi^i \right) & \text{for KLaS} \end{cases} \quad (4)$$

where B^i is the Langmuir constant of component g^i in 1/Pa (Pan et al., 2008), and Y^i is the dimensionless mole fraction of the gas component i in the water-free gas phase. Note that the T+GW and T+G codes offer the additional options of linear and Freundlich sorption isotherms (equilibrium and kinetic). These are described by the following equations:

$$\begin{cases} \Psi^i = K_l^i \, p^i & \text{for ELiS} \\ \dfrac{d\Psi^i}{dt} = k_l^i \left(K_l^i \, p^i - \Psi^i \right) & \text{for KLiS} \end{cases} \quad (5)$$

$$\begin{cases} \Psi^i = K_F^i \, \left(p^i \right)^c & \text{for EFS} \\ \dfrac{d\Psi^i}{dt} = k_F^i \left[K_F^i \, \left(p^i \right)^c - \Psi^i \right] & \text{for KFS} \end{cases} \quad (6)$$

where ELiS and KLiS denote equilibrium and kinetic linear sorption, respectively; EFS and KFS denote equilibrium and kinetic Freundlich sorption, respectively; K^i_l and K^i_F are the distribution coefficients of the ELiS and EFS sorption isotherms of gas component i, respectively; p^i is the partial pressure of i; k^i_l and k^i_F are the kinetic coefficients of the ELiS and EFS sorption isotherms of i, respectively; and c is the exponent of the Freundlich sorption isotherm.

Heat accumulation terms

The heat accumulation term includes contributions from the rock matrix and all the phases, and is given by the equation

$$M^\theta = \begin{cases} (1-\phi)\rho_R \int_{T_0}^{T} C_R(T)\, dT + \\ \sum_{\beta=A,G} \phi S_\beta \rho_\beta U_\beta + \delta_\Psi (1-\phi)\rho_R \sum_{i=1}^{N_G} u^i Y^i \end{cases} \quad (7)$$

where $C_R = C_R(T)$ is the heat capacity of the dry rock [J kg^{-1} K^{-1}]; U_β is the specific internal energy of phase β [J kg^{-1}]; u^i is the specific internal energy of sorbed gas component i [J kg^{-1}]; T is the temperature [K]; and T_0 is a reference temperature [K]. The specific internal energy of the gaseous phase is a very strong function of composition, is related to the specific enthalpy of the gas phase H_G, and is given by

$$U_G = \sum_{\kappa=w,g^i(i=1,N_G)} X_G^\kappa \, u^\kappa + U_{dep} \quad \left(= H_G - \frac{P}{\rho_G} \right) \quad (8)$$

where u^κ is the specific internal energy of component κ in the gaseous phase, and U_{dep} is the specific internal energy departure of the gas mixture [J kg^{-1}]. The internal energy of the aqueous phase accounts for the effects of gas and inhibitor solution, and is estimated from

$$U_A = X_A^w u^w + \sum_{i=1}^{N_G} X_A^{g^i} \left(u^i + U^i_{sol} \right) \quad (9)$$

where u^w and u^i are the specific internal energies of H_2O and of natural gas component i at the P and T conditions of the aqueous phase, respectively, and U^i_{sol} are the specific internal energies of dissolution of the gas component i in H_2O.

Fluid flow terms

The mass fluxes of water and of the gaseous components include contributions from the aqueous and gaseous phases, i.e.,

$$\mathbf{F}^\kappa = \sum_{\beta=A,G} \mathbf{F}^\kappa_\beta, \; \kappa \equiv w, g^i, \; i = 1,...,N_G \quad (10)$$

For phase β, $\mathbf{F}^\kappa_\beta = X^\kappa_\beta \, \mathbf{F}_\beta$. In T+GW and T+G, there are three options to describe the phase flux $\mathbf{F}_\beta$. The first is the standard Darcy's law, i.e.,

$$\mathbf{F}_\beta = \rho_\beta \left[-\frac{k \, k_{r\beta}}{\mu_\beta} \nabla \Phi_\beta \right] = \rho_\beta \mathbf{v}_\beta, \;\; \nabla \Phi_\beta = \nabla P_\beta - \rho_\beta \mathbf{g}, \quad (11)$$

where k is the rock intrinsic permeability [m^2]; $k_{r\beta}$ is the relative permeability of phase β [dimensionless]; μ_β is the viscosity of phase β [Pa s]; P_β is the pressure of the aqueous phase [Pa]; and $\mathbf{g}$ is the gravitational acceleration vector [m s^{-2}]. In T+GW, the relationship between the aqueous and the gas pressures, P_A and P_G, respectively, is given by $P_A = P_G + P_{cGA}$, where P_{cGA} is the gas-water capillary pressure [Pa]. The P_{cGA} options are the standard ones available in the TOUGH2 and TOUGH+ family of codes (Pruess et al., 1999; Moridis et al., 2008).

The mass flux of component κ in the gas phase incorporates advection and diffusion contributions, and is given by

$$\mathbf{F}^\kappa_G = \left(1 + \frac{b}{P_G} \right) \rho_G \mathbf{v}_G X^\kappa_G \underbrace{- \phi S_G \tau_G D^\kappa_G \rho_G \nabla X^\kappa_G}_{-\mathbf{J}^\kappa_G}, \quad (12)$$

where b is the *Klinkenberg* (1941) b-factor accounting for gas slippage effects [Pa], the term $\boldsymbol{J}^k_G$ is the diffusive mass flux of component κ in the gas phase [kg m^{-2} s^{-1}], D^k_G is the multicomponent molecular diffusion coefficient of component k in the gas phase in the absence of a porous medium [m^2 s^{-1}], and τ_G is the gas tortuosity [dimensionless]. There are several methods to compute τ_G in the T+GW and T+G codes, including the Millington and Quirk [1961] model. The diffusive mass fluxes of the water vapor and the natural gas components are related through the relationship of Bird et al. (2007)

$$\mathbf{J}^w_G + \sum_{i=1}^{N_G} \mathbf{J}^{g^i}_G = 0, \quad (13)$$

which ensures that the total diffusive mass flux of the gas phase is zero with respect to the mass average velocity when summed over the components. Then the total mass flux of the gas phase is the product of its velocity and density.

If the flow is non-Darcian, then the equation $\mathbf{F}_\beta = \rho_\beta \mathbf{v}_\beta$ still applies, but $\mathbf{v}_\beta$ is now computed from the solution of the quadratic equation

$$\nabla\Phi_\beta = -\left(\frac{\mu_\beta}{k\, k_{r\beta}} \mathbf{v}_\beta + \beta_\beta \rho_\beta \mathbf{v}_\beta \left| \mathbf{v}_\beta \right| \right), \quad (14)$$

in which β_β is the "turbulence correction factor" (Katz et al., 1959). The quadratic equation in (14) is the general momentum-balance *Forcheimer equation* (Forchheimer, 1901; Wattenbarger and Ramey, 1968), and incorporates laminar, inertial and turbulent effects. This is the second option. The solution then is

$$\mathbf{v}_\beta = \frac{2\nabla\Phi_\beta}{\dfrac{\mu_\beta}{k\, k_{r\beta}} + \sqrt{\left(\dfrac{\mu_\beta}{k\, k_{r\beta}} \right)^2 + 4\beta_\beta \rho \left| \nabla\Phi_\beta \right|}}, \quad (15)$$

and $\mathbf{v}_\beta$ from equation (15) is then used in the equations of flow (11) and (12). T+GW and T+G offer 13 options to compute β_β, several of which are listed in Finsterle (2001). The third option follows the approach of Barree and Conway (2007), as described by Wu et al. (2011), which involves a different formulation of $\nabla\Phi_\beta$.

The Klinkenberg b-factor is either provided as input, or is computed using the relationship proposed by Jones (1972) as

$$\frac{b}{b_0} = \left(\frac{k}{k_0} \right)^{-0.36}, \quad (16)$$

where the subscript 0 denotes a reference medium with a known b-factor and k, such as those listed by Wu et al. (1998).

Micro-flow: Knudsen diffusion and Dusty Gas model

For ultra-low permeability media (such as tight sands and shales) and the resulting micro-flow processes, the Klinkenberg b-factor for a single-component or pseudo-component gas in T+GW and T+G is computed by the method of Florence et al. (2007) and Freeman et al. (2011) as

$$\frac{b}{P_G} = \left(1 + \alpha K_n\right)\left(1 + \frac{4K_n}{1 + K_n}\right) - 1, \quad (17)$$

where K_n is the Knudsen diffusion number (dimensionless), which characterizes the deviation from continuum flow, accounts for the effects of the mean free path of gas molecules being on the same order as the pore dimensions of the porous media, and is computed from (Freeman et al., 2011) as

$$K_n = \frac{\bar{\lambda}}{r_{pore}} = \frac{\mu_G}{2.81708 P_G} \sqrt{\frac{\pi RT}{2M}} \frac{\phi}{k}, \quad (18)$$

with M being the molecular weight and T the temperature (°K). The term α is determined from Karniadakis and Beskok (2001) as

$$\alpha = \frac{128}{15\pi^2} \tan^{-1}\left(4K_n^{0.4}\right), \quad (19)$$

For simplicity, we have omitted the i superscript in equations (16) to (19). The Knudsen diffusion can be very important in porous media with very small pores (on the order of a few micrometers or smaller) and at low pressures. For a single gas pseudo-component, the properties in (16) are obtained from an appropriate equation of state for a real-gas mixture of constant composition Y^i. The Knudsen diffusivity D_K [m^2/s] can be computed as (Civan, 2008; Freeman et al., 2011)

$$D_K = \frac{4\sqrt{k\phi}}{2.81708} \sqrt{\frac{\pi RT}{2M}} \quad \text{or} \quad D_K = \frac{kb}{\mu_G} \quad (20)$$

For a multicomponent gas mixture that is not treated as a single pseudo-component, ordinary Fickian diffusion must be taken into account as well as Knudsen diffusion**.** Use of the advective–diffusive flow model (Fick's law) should be restricted to media with $k \geq 10^{-12}$ m^2; the dusty-gas model (DGM) is more accurate at lower k

(Webb and Pruess, 2003). Additionally, DGM accounts for molecular interactions with the pore walls in the form of Knudsen diffusion. Shales may exhibit k as low as 10^{-21} m^2, so the DGM described below is more appropriate than the Fickian model (Webb and Pruess, 2003; Doronin and Larkin 2004; Freeman et al., 2011):

$$\left.\begin{aligned}\sum_{j=1,j\neq i}^{N_G}\frac{Y^i N_D^j - Y^j N_D^i}{D_e^{ij}} - \frac{N_D^i}{D_K^i} = \\ \frac{p^i \nabla Y^i}{ZRT} + \left(1+\frac{kp}{\mu_G D_K^i}\right)\frac{Y^i \nabla p^i}{ZRT}\end{aligned}\right\}, \quad (21)$$

where N^i_D is the molar flux of component i in mole/m^2/s, D_e^{ij} is the effective gas (binary) diffusivity of species i in species j, D_K^i is the Knudsen diffusivity of species i.

Gas solubility

There are two options for estimating the solubility of a gas i into the aqueous phase in T+GW. The first (and simpler one) is based on Henry's Law, described by the relationship

$$p^i = H^i X_A^i, \quad (22)$$

where H^i [Pa] is referred to as Henry's factor and is a T-dependent, species-specific factor (thus, it cannot be called Henry's *constant*). T+GW includes a library of fast parametric relationships of $H^i = H^i(\mathrm{T})$, and this is the preferred option if a single gas component or pseudo-component is involved. The second option is based on the equality of fugacities in the aqueous and the gas phase, and involves the chemical potentials of the various species in solution.

Heat flux

The heat flux accounts for conduction, advection and radiative heat transfer, and is given by

$$\mathbf{F}^\theta = -\bar{k}_\theta \nabla T + f_\sigma \sigma_0 \nabla T^4 + \sum_{\beta\equiv A,G} h_\beta \mathbf{F}_\beta, \quad (23)$$

where $\bar{k}_\theta$ is a representative thermal conductivity of the fluid-impregnated rock [W m^{-1} K^{-1}]; h_b is a specific enthalpy of phase β [J kg^{-1}]; f_σ is the radiance emittance factor [dimensionless]; σ_0 is the Stefan-Boltzmann constant [5.6687×10^{-8} J m^{-2} K^{-4}]. The specific enthalpy of the gas phase is computed as

$$H_G = \sum_{\kappa\equiv w,g_i} X_G^\kappa h_G^\kappa + H_{dep}, \quad (24)$$

where h_G^κ is the specific enthalpy of component k in the gaseous phase, and H_{dep} is the specific enthalpy departure of the gas mixture [J kg^{-1}]. The specific enthalpy of the aqueous phase is estimated from

$$H_A = X_A^w h_A^w + \sum_i X_A^{g^i}\left(h_A^{g^i} + H_{sol}^{g^i}\right), \quad (25)$$

where h_A^w and $h_A^{g^i}$ are the specific enthalpies of H_2O and of the natural gas components in the aqueous phase, respectively, and $H_{sol}^{g^i}$ is the specific enthalpy of dissolution [J kg^{-1}] of gas component g^i in the aqueous phase.

Source and sink terms. In sinks with specified mass production rate, withdrawal of the mass component k is described by

$$\hat{q}^\kappa = \sum_{\kappa\equiv A,G} X_\beta^\kappa q_\beta, \quad \kappa = \mathrm{w}, g^i \ (i = 1,...,N_G), \quad (26)$$

where q_β is the production rate of the phase b [kg m^{-3}]. For a prescribed production rate, the phase flow rate q_β is determined from the phase mobility at the location of the sink. For source terms (well injection), the addition of a mass component k occurs at desired rates.

Thermophysical properties

The water properties in the T+GW code are obtained from steam table equations (Pruess et al., 1999; Moridis et al., 2008). All the real gas properties in T+G and T+GW are computed from one of the three available options of cubic equations of state that were first developed for TOUGH+HYDRATE (Moridis et al., 2008).

Solution approach

The fully implicit discretized nonlinear balance equations are expressed in residual form, are then linearized by the Newton-Raphson method, and the resulting Jacobian is solved in the standard approach used in all TOUGH applications (Pruess et al., 1999). In T+G, the primary variables that constitute the solution vector are p, Y^i (i = 1,…, N_G), and T; in T+GW, the primary variables are the same for single-phase gas; p, X^i_A and T for single-phase aqueous conditions, and S_A, Y^i and T for two-phase conditions.

VALIDATION EXAMPLES

Problem V1: Real gas flow in a cylindrical reservoir

Using the concept of pseudo-pressure, Fraim and Wattenbarger (1986) developed a solution to the

problem of transient flow in a finite cylindrical real-gas reservoir with a producing well at its center, described as:

$$p_D = \frac{1}{2} E_i\left(\frac{r_D^2}{4t_D}\right), \quad (27)$$

where E_i denotes the exponential integral,

$$p_D = \frac{kh}{q_V B\mu}(\psi_0 - \psi),\ r_D = \frac{r}{r_w},\ t_D = \frac{k}{\phi\mu c_t r_w^2}t,\ \psi = 2\int_{p_r}^{p}\frac{p}{\mu z}dp,$$

ψ is the pseudo-pressure, r is the radius, r_w is the well radius [m], p_r is a reference pressure [Pa], c_t is the total compressibility [Pa^{-1}], q_V is the volumetric production rate [ST m^3/s], B is the formation volume factor, h is the reservoir thickness, and the subscript 0 indicates the initial conditions. The data used in the simulation of this validation problem appear in Table 1. The domain discretization involved logarithmically increasing Δr's. Figure 1 shows an excellent agreement of the analytical and the T+GW numerical solutions at various sampling times. The T+G code yields an identical solution.

Table 1. Properties and conditions in Problem V1.

Data Type	Values
Matrix permeability k	$3.04\text{x}10^{-14}$ m^2 (30.4 mD)
Reservoir thickness h	10 m
Well radius r_w	0.059 m
Reservoir radius r_e	100 m
Reservoir pressure p	10 MPa
Reservoir temperature T	60 °C
Reservoir porosity ϕ	0.30
Rock compressibility	$2\text{x}10^{-10}$ 1/Pa
Gas composition	100% CH_4
Gas EOS	Peng-Robinson

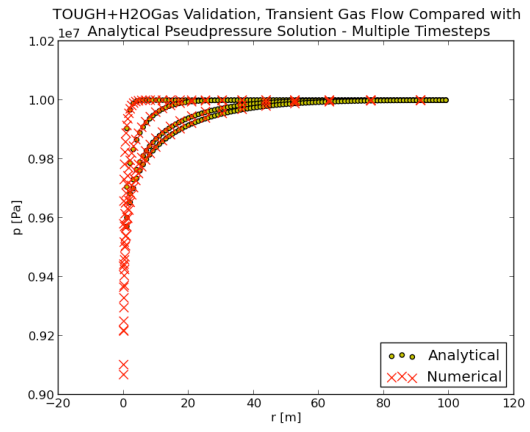

Figure 1. Comparison of the analytical and the T+GW solutions in problem V1.

Problem V2: Water flow in a cylindrical reservoir

Blasingame (1993) developed an analytical solution of pseudo-steady state flow in a circular reservoir with a producing well at its center and impermeable boundaries at $r=r_e$. Using the data listed in Table 2, the T+GW solution in Figure 2 (based on a grid with logarithmically increasing Δr's) practically coincides with the analytical solution, increasing confidence in the code.

Table 2. Properties and conditions in Problem V2.

Data Type	Values
Matrix permeability k	$3.04\text{x}10^{-14}$ m^2 (30.4 mD)
Reservoir thickness h	10 m
Well radius r_w	0.059 m
Reservoir radius r_e	100 m
Reservoir pressure p	10 MPa
Reservoir temperature T	30 °C
Reservoir porosity ϕ	0.30
Total compressibility c_t	$4.88\text{x}10^{-10}$ 1/Pa
Gas EOS	Peng-Robinson

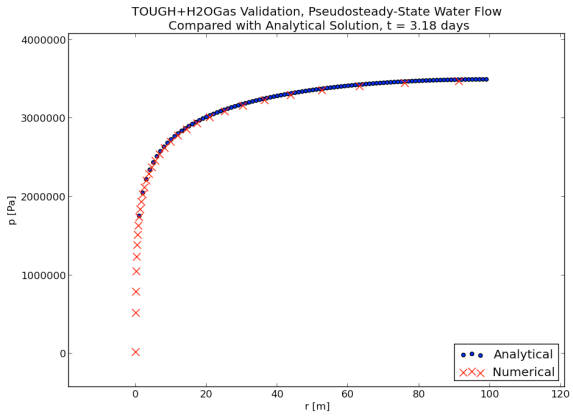

Figure 2. Problem V2: Comparison of the analytical and the T+GW solutions at t = 3.18 days.

Problem V3: Gas flow in a tight gas reservoir with vertical well intersecting a vertical fracture plane

Cinco-Ley et al. (1978) proposed an analytical solution to the problem of a gas flow in a low-permeability 'slab' of a gas reservoir (i.e., with infinite-acting boundaries), in which a vertical well intersects the middle axis of a vertical planar fracture. Treating the "slab" reservoir as a single layer, we solved the same problem numerically using a 2D domain with sufficiently long dimensions to satisfy the infinite-acting

boundary conditions during the simulation period. From the data in Table 3, this is an ultra-tight fractured reservoir with no gas sorption.

The numerical solutions from the T+G and T+GW codes are identical. The point pressure results in Figure 3 identify the element centers and shows the very fine discretization (beginning from mm-scale) in the vicinity of the fracture. The contour plot of the pressure distribution at t = 2.13 years (Figure 4) clearly shows the effect of the fracture and the resulting flow pattern. The log-log plot of production rate vs. time in Figure 5 includes the fully coinciding analytical and numerical solutions, and exhibits the typical -½ slope of vertically fractured reservoirs under production.

Table 3. Properties and conditions in Problem V1.

Data Type	Values
Matrix permeability k	3.08×10^{-19} m^2 (30.8 nD)
Fracture permeability k_f	6.68×10^{-14} m^2 (0.668 D)
Fracture half-length	20 m
Reservoir thickness h	10 m
Well radius r_w	0.05 m
Well pressure p_w	5 MPa
Reservoir pressure p	10 MPa
Reservoir temperature T	60 °C
Reservoir porosity ϕ	0.10
Rock compressibility	2×10^{-10} 1/Pa
Gas composition	100% CH_4
Gas EOS	Peng-Robinson

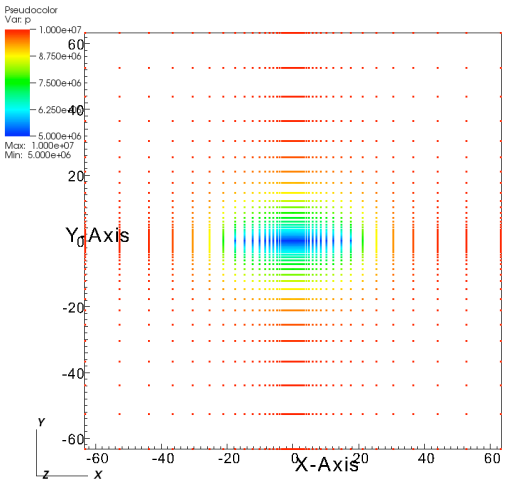

Figure 3. Point cloud of pressure distribution at t = 2.13 years in problem V3, indicating discretization.

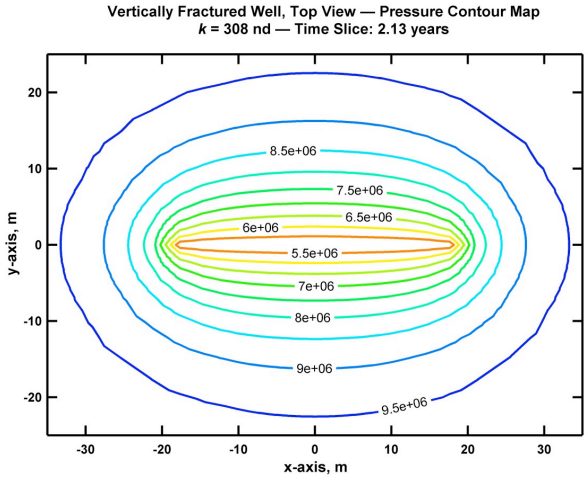

Figure 4. Pressure dustribution in the tight gas reservoir in Problem V3 (T+G and T+GW solutions).

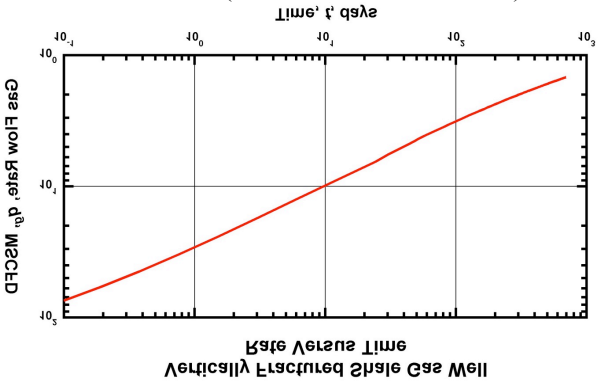

Figure 5. Gas production rate at the well in Problem V3 (coinciding analytical, T+G and T+GW solutions).

APPLICATION EXAMPLES

Problem A1: Gas production from a shale gas reservoir using a horizontal well

This T+G study focuses on a Cartesian 3D stencil of a horizontal well section that is typical of a Type I shale gas system (Figure 6), as defined and investigated by Freeman (2010) and Moridis et al. (2010). Such systems involve the (usually hydraulically) induced primary fractures (PF), the undisturbed matrix, and the stress release fractures around the well. The data used in this simulation were as in Freeman (2010). The surface area of the Cartesian system at the well was corrected to reflect its cylindrical geometry. The discretization involved subdivisions as small as mm-scale near the fracture face, and resulted in about 800,000 gridblocks. The gas was 100% CH_4. The predicted production rate when the well is operated at a constant bottomhole pres-

sure P_w is shown in Figure 7, which also lists some of the data used in the simulation. Note that here, and in Problem A2, dimensioneless variables are used, which are defined as:

$$t_D = 0.0002637 \frac{k}{\phi \mu c_t x_f^2} \frac{1}{[1+(0.00525)V_L]} t \quad \text{(28)}$$

$$q_D = 141.2 \frac{B\mu}{kh(p_i - p_{wf})} q \quad \text{(29)}$$

The T+GW results were identical.

Problem A2: Gas production from a shale gas reservoir with a complex fracture system using a horizontal well

Problem A2 is a sensitivity analysis study that aims to determine the effects of more complex fracture regimes. These are represented by Types II, III and IV (Figure 8), which include secondary planar fractures (perpendicular to the primary fractures), natural fractures, and all types of fractures, respectively. Type IV is the most complex system to describe, simulate and analyze. The data in these simulations were as in Freeman (2010). The natural fractures were described by a dual-porosity model using the MINC concept, and the secondary fractures were represented as individual sub-domains.

The T+G and T+GW results in Figure 9 (which include the Type I predictions for reference) confirm the importance of the additional fractures on production. Type IV exhibits the highest early production because of its maximum surface area and the largest number of flow pathways to the well, but also among the fastest production declines because of exhaustion of the gas and its slow replenishment from sorption. The other types exhibit intermediate behavior.

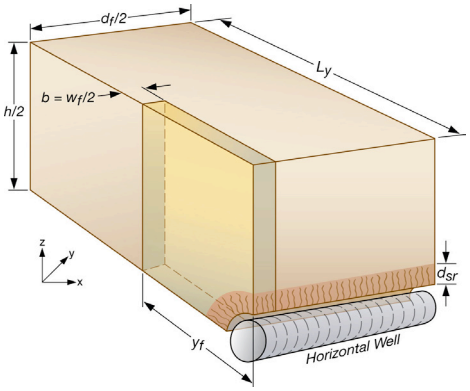

Figure 6. Stencil of a Type I system involving a horizontal well in a tight- or shale-gas reservoir (Moridis et al., 2010).

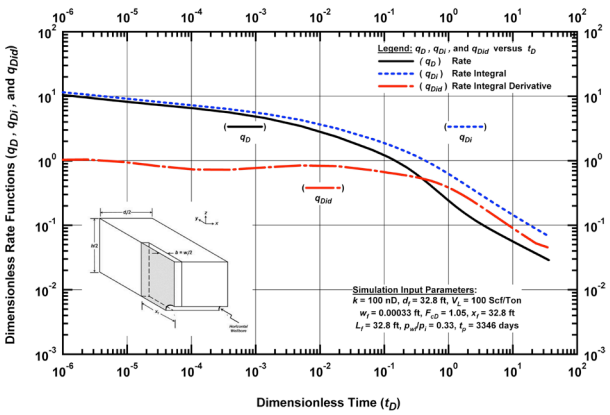

Figure 7. Prediction of gas production in Problem A1 (Freeman et al., 2010).

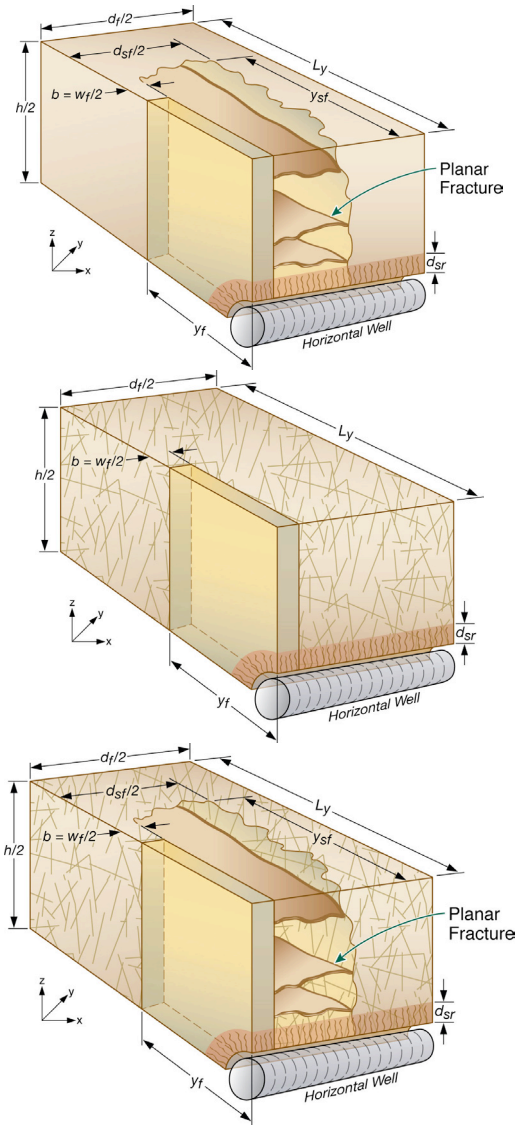

Figure 8. Stencils of Type II, III and IV systems involving a horizontal well in a tight- or shale-gas reservoir (Moridis et al., 2010).

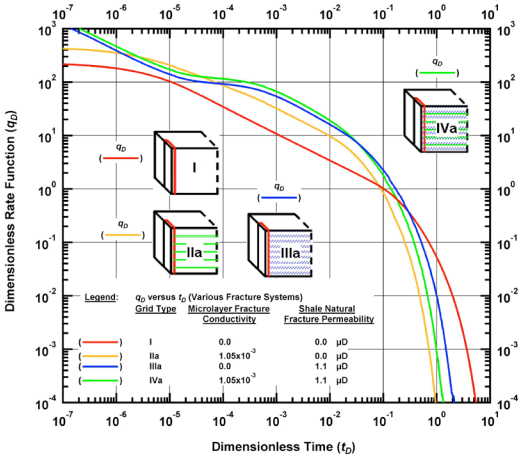

Figure 9. Effect of fracture regime on gas production in Problem A2 (Freeman et al., 2010).

Problem A3: Flowing gas composition changes in shale gas wells

Here we investigate compositional changes over time in gas produced from a shale reservoir. The initial gas composition was: Y = 80% CH_4, 7% C_2H_6, 5% C_3H_8, 5% C_4H_{10}, 2% C_5H_{12} and 1% C_6H_{16}. A Type I system was assumed. The system characteristics, properties and conditions are as described in Freeman et al. (2012). Gas was produced by maintaining the well at a constant bottomhole pressure.

The identical T+G and T+GW results in Figure 10 include both (a) the flow rate, which shows the slope of -½ typical of fractured shale reservoirs, and (b) the compositional deviation of the produced gas over time, which clearly shows inflection points correlating perfectly with the times at which significant changes occur in the gas flow regime in the shale.

SUMMARY

We discuss the T+G and T+GW additions to the TOUGH+ family of codes. T+GW describes the non-isothermal two-phase flow of water and a real gas mixture of up to 9 components in a gas reservoir (including a tight/shale gas one), and accounts for coupled flow and thermal effects in porous and/or fractured media, real gas behavior, inertial (Klinkenberg) effects, full microflow treatment, Darcy and non-Darcy flow through the matrix and fractures of fractured media, gas sorption onto the grains of the porous media, etc. T+G has the same general capabilities, but does not include water, thus describing a single-phase, dry-gas system.

We validate the codes against available analytical and semi-analytical solutions. We show the code capabilities in a series of problems of increasing complexity, ranging from isothermal flow in simpler 1D and 2D conventional gas reservoirs, to non-isothermal gas flow in 3D fractured shale gas reservoirs involving multiple types of fractures, micro-flow, non-Darcy flow and gas composition changes during production.

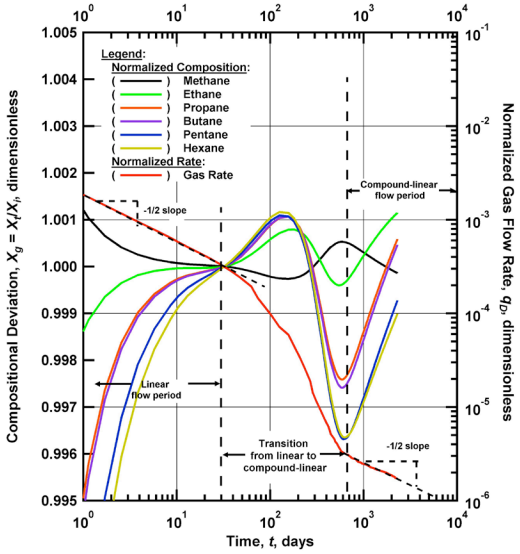

Figure 10. Prediction of gas production and compositional changes in Problem A3 (Freeman et al., 2012).

ACKNOWLEDGMENT

The research described in this article has been funded by the U.S. Environmental Protection Agency through Interagency Agreement (DW-89-92235901-C) to the Lawrence Berkeley National Laboratory, and by the Research Partnership to Secure Energy for America (RPSEA - Contract No. 08122-45) through the Ultra-Deepwater and Unconventional Natural Gas and Other Petroleum Resources Research and Development Program as authorized by the US Energy Policy Act (EPAct) of 2005. The views expressed in this article are those of the author(s) and do not necessarily reflect the views or policies of the EPA.

REFERENCES

Barree R.D., and M.W. Conway, Multuiphase non-Darcy flow in proppant packs, Paper SPE 109561, 2007 Annual Technical Conference and Exhibition, Anaheim, CA, 11–14 Nov 2007.

Bird, R.B., W.E. Stewart, and E.N. Lightfoot, *Transport Phenomena*. New York: John Wiley & Sons, Inc., 2007.

Blasingame, T.A., Semi-Analytical Solutions for a Bounded Circular Reservoir – No Flow and Constant Pressure Outer Boundary Conditions: Unfractured Well Case, Paper SPE 25479, SPE Production Operations Symposium, Oklahoma City, Oklahoma, 21-23 March 1993.

Cinco-Ley, H., F. Samaniego, and N. Dominguez, Transient pressure behavior for a well with a finite-conductivity vertical fracture, *SPE Journal* 18 (4): 253-264. SPE 6014-PA. http://dx.doi.org/10.2118/6014-PA

Civan, F., Effective Correlation of Apparent Gas Permeability in Tight Porous Media. *Transp. in Porous Med*., 2008., DOI: 10.1007/s11242-009-9432-z

Clarkson, C.R. and R.M. Bustin, Binary gas adsorption/desorption isotherms: effect of moister and coal composition upon carbon dioxide selectivity over methane. *International Journal of Coal Geology*, 42, 241-271, 1999.

Doronin, G.G. and N.A. Larkin, On dusty gas model governed by the Kuramoto-Sivashinsky equation. *Computational and Applied Mathematics, 23*(1), 67-80, 2004

Finsterle, S., Implementation of the Forchheimer Equation in iTOUGH2, Project Report, Lawrence Berkeley National Laboratory, Berkeley, Calif., 2001.

Fraim, M.L., and R.A. Wattenbarger, Gas Reservoir Decline Curve Analysis Using Type Curves with Real Gas Pseudopressure and Pseudotime, *SPEFE*, 671-682, 1987.

Freeman, C.M., Study of flow regimes in multiply-fractured horizontal wells in tight gas and shale gas reservoir systems, M.Sc. Thesis, Petroleum Engineering Department, Texas A&M University, 2010.

Freeman, C.M., G.J. Moridis, and T.A. Blasingame, A Numerical Study of Microscale Flow Behavior in Tight Gas and Shale Gas Reservoir Systems. *Transp. in Porous Med., 90*(1): 253-268, 2011, doi:10.1007/s11242-011-9761-6

Freeman, C.M., G.J. Moridis, E. Michael, and T.A. Blasingame, Measurement, Modeling, and Diagnostics of Flowing Gas Composition Changes in Shale Gas Wells, Paper SPE 153391, SPE Latin American and Caribbean Petroleum Engineering Conference, Mexico City, Mexico, 16-18 April, 2012.

Forchheimer, P., Wasserbewewegung durch Boden, *ZVDI* 45, 1781, 1901.

Gao, C., J.W. Lee, J.P. Spivey, and M.E. Semmelbeck, Modeling multilayer gas reservoirs including sorption effects, SPE paper 29173, SPE Eastern Regional Conference & Exhibition, Charleston, West Virginia, 8-10 November, 1994.

Jones, S. C., A rapid accurate unsteady-state Klinkenberg parameter, *SPE Journal* 383–397, 1972.

Katz, D. L. et al., *Handbook of Natural Gas Engineering*, McGraw-Hill, New York, 1959.

Klinkenberg, L.J., The Permeability of Porous Media to Liquid and Gases, Proceedings, *API Drilling and Production Practice*, 200-213, 1941.

Millington, R.J., and J.P. Quirk, Permeability of porous solids. *Trans. Faraday Soc*. 57, 1200-1207, 1961.

Moridis, G.J., M. Kowalsky and K. Pruess. TOUGH+HYDRATE v1.0 User's Manual. LBNL-161E, Lawrence Berkeley National Laborotory, Berkeley, Calif., 2008.

G.J. Moridis, T.A. Blasingame, and C.M. Freeman, Analysis of Mechanisms of Flow in Fractured Tight-Gas and Shale-Gas Reservoirs, Paper SPE 139250, SPE Latin American & Caribbean Petroleum Engineering Conference, Lima, Peru, 1–3 December 2010.

Pruess, K., C. Oldenburg, and G. Moridis, *TOUGH2 User's Guide, Version 2.0*, Report LBNL-43134, Lawrence Berkeley National Laboratory, Berkeley, Calif., 1999.

Schettler, P.D., and C.R. Parmely, Contributions to total storage capacity in devonian shales, SPE paper 23422, SPE Eastern Regional Meeting, Lexington, Kentucky, 22-25 October, 1991.

Wattenbarger, R.A. and H.J. Ramey, Gas well testing with turbulence, damage and wellbore storage, SPE 1835, *J. Pet. Tech.*, 877-884, 1968.

Webb, S.W. and K. Pruess, The Use of Fick's Law for Modeling Trace Gas Diffusion in Porous Media. *Transport in Porous Media, 51,* 327-341, 2003.

Wu, Y.S., B. Lai, J.L. Miskimins, P. Fakcharoenphol and Y. Di, Analysis of Multiphase Non-Darcy Flow in Porous Media, Transport in Porous Media, (2011) 88, 205–223, 2011,DOI 10.1007/s11242-011-9735-8